Development/Plasticity/Repair

Longitudinal Allometry of Sulcal Morphology in Health and Schizophrenia

Joost Janssen,[1,2,3,4] Clara Alloza,[1,2,3] Covadonga M. Díaz-Caneja,[1,2,3,5] Javier Santonja,[1,2] Laura Pina-Camacho,[1,2,3,5] Pedro M. Gordaliza,[6] Alberto Fernández-Pena,[2,6] Noemi González Lois,[1,2] Elizabeth E.L. Buimer,[4] Neeltje E.M. van Haren,[4,7] Wiepke Cahn,[4] Eduard Vieta,[3,9] Josefina Castro-Fornieles,[3,10] Miquel Bernardo,[3,8] Celso Arango,[1,2,3,5] René S. Kahn,[4,11] Hilleke E. Hulshoff Pol,[4] and Hugo G. Schnack[4]

[1]Department of Child and Adolescent Psychiatry, Institute of Psychiatry and Mental Health, Hospital General Universitario Gregorio Marañón, 28007 Madrid, Spain, [2]Instituto de Investigación Sanitaria Gregorio Marañón, 28007 Madrid, Spain, [3]Ciber del Área de Salud Mental, 28007 Madrid, Spain, [4]Department of Psychiatry, UMCU Brain Center, University Medical Center Utrecht, 3584 CX Utrecht, The Netherlands, [5]School of Medicine, Universidad Complutense, 28040 Madrid, Spain, [6]Departamento de Bioingeniería e Ingeniería Aeroespacial, Universidad Carlos III de Madrid, 28911 Madrid, Spain, [7]Department of Child and Adolescent Psychiatry/Psychology, Erasmus University Medical Centre, Sophia Children's Hospital, 3015 GD Rotterdam, The Netherlands, [8]Barcelona Clinic Schizophrenia Unit, Hospital Clinic of Barcelona, Neuroscience Institute, Institut d'Investigacions Biomèdiques August Pi i Sunyer, University of Barcelona, 08036 Barcelona, Spain, [9]Bipolar Disorders Unit, Clinical Institute of Neurosciences, Hospital Clínic, University of Barcelona, Institut d'Investigacions Biomèdiques August Pi i Sunyer, 08036 Barcelona, Spain, [10]Department of Child and Adolescent Psychiatry and Psychology, Clinical Institute of Neurosciences, Hospital Clínic, University of Barcelona, Institut d'Investigacions Biomèdiques August Pi i Sunyer, 08036 Barcelona, Spain, and [11]Department of Psychiatry, Icahn School of Medicine at Mount Sinai, 10029 New York

Scaling between subcomponents of folding and total brain volume (TBV) in healthy individuals (HIs) is allometric. It is unclear whether this is true in schizophrenia (SZ) or first-episode psychosis (FEP). This study confirmed normative allometric scaling norms in HIs using discovery and replication samples. Cross-sectional and longitudinal diagnostic differences in folding subcomponents were then assessed using an allometric framework. Structural imaging from a longitudinal (Sample 1: HI and SZ, $n_{HI\ Baseline} = 298$, $n_{SZ\ Baseline} = 169$, $n_{HI\ Follow\text{-}up} = 293$, $n_{SZ\ Follow\text{-}up} = 168$, totaling 1087 images, all individuals ≥ 2 images, age 16-69 years) and a cross-sectional sample (Sample 2: $n_{HI} = 61$ and $n_{FEP} = 89$, age 10-30 years), all human males and females, is leveraged to calculate global folding and its nested subcomponents: sulcation index (SI, total sulcal/cortical hull area) and determinants of sulcal area: sulcal length and sulcal depth. Scaling of SI, sulcal area, and sulcal length with TBV in SZ and FEP was allometric and did not differ from HIs. Longitudinal age trajectories demonstrated steeper loss of SI and sulcal area through adulthood in SZ. Longitudinal allometric analysis revealed that both annual change in SI and sulcal area was significantly stronger related to change in TBV in SZ compared with HIs. Our results detail the first evidence of the disproportionate contribution of changes in SI and sulcal area to TBV changes in SZ. Longitudinal allometric analysis of sulcal morphology provides deeper insight into lifespan trajectories of cortical folding in SZ.

Key words: **allometry; cortical folding; first-episode psychosis; longitudinal; schizophrenia; sulcus**

Received Mar. 11, 2021; revised Feb. 24, 2022; accepted Mar. 1, 2022.

Author contributions: J.J., M.B., and H.G.S. designed research; J.J. and H.G.S. performed research; J.J., J.S., P.M.G., and H.G.S. analyzed data; J.J. and H.G.S. wrote the first draft of the paper; J.J., C. Alloza, C.M.D.-C., L.P.-C., P.M.G., A.F.-P., N.G.L., E.E.L.B., N.E.M.v.H., W.C., E.V., J.C.-F., C. Arango, R.S.K., H.E.H.P., and H.G.S. edited the paper; J.J., C.M.D.-C., R.S.K., H.E.H.P., and H.G.S. wrote the paper.

This work was supported by the Spanish Ministry of Science and Innovation, Instituto de Salud Carlos III (PI17/01249, PI17/00997, PI19/01024, PI20/00721, PI08/0208, PI11/00325, PI14/00612), cofinanced by European Regional Development Fund from the European Commission, "A way of making Europe," Ciber del Área de Salud Mental, Madrid Regional Government (B2017/BMD-3740 AGES-CM-2), European Union Structural Funds, European Union Seventh Framework Program under Grant Agreements FP7-HEALTH-2009-2.2.1-2-241909 (Project EU-GEI), FP7-HEALTH-2009-2.2.1-3-242114 (Project OPTiMISE), FP7- HEALTH-2013-2.2.1-2-603196 (Project PSYSCAN), and FP7-HEALTH-2013-2.2.1-2-602478 (Project METSY); and European Union H2020 Program under the Innovative Medicines Initiative 2 Joint Undertaking (Grant Agreement 115916, Project PRISM, and Grant Agreement 777394, Project AIMS-2-TRIALS), Fundación Familia Alonso, Fundación Alicia Koplowitz, and Fundación Mutua Madrileña. C.M.D.-C. holds a Juan Rodés grant from Instituto de Salud Carlos III (JR19/00024). This work has been performed thanks to the 3T Equipment of Magnetic Resonance at Institut d'Investigacions Biomèdiques August Pi i Sunyer (project IBPS15-EE-3688 cofunded by Ministerio de Ciencia, Innovación y Universidades (MCIU) and by European Regional Development Fund). We thank Zimbo Boudewijns, Joyce van Baaren, and Diego Muñoz Beltrán for technical assistance.

C.M.D.-C. has received fees from AbbVie, Sanofi, and Exeltis. C. Arango has been a consultant to or has received honoraria or grants from Acadia, Angelini, Gedeon Richter, Janssen-Cilag, Lundbeck, Otsuka, Roche, Sage, Servier, Shire, Schering-Plough, Sumitomo Dainippon Pharma, Sunovion, and Takeda. W.C. has received unrestricted research grants from or served as an independent symposium speaker or consultant for Eli Lilly, Bristol-Myers Squibb, Lundbeck, Sanofi-Aventis, Janssen-Cilag, AstraZeneca, and Schering-Plough. The remaining authors declare no competing financial interests.

Correspondence should be addressed to Joost Janssen at joost.janssen76@gmail.com.

https://doi.org/10.1523/JNEUROSCI.0606-21.2022

Significance Statement

Psychotic disorders are associated with deficits in cortical folding and brain size, but we lack knowledge of how these two morphometric features are related. We leverage cross-sectional and longitudinal samples in which we decompose folding into a set of nested subcomponents: sulcal and hull area, and sulcal depth and length. We reveal that, in both schizophrenia and first-episode psychosis, (1) scaling of subcomponents with brain size is different from expected scaling laws and (2) caution is warranted when interpreting results from traditional methods for brain size correction. Longitudinal allometric scaling points to loss of sulcal area as a principal contributor to loss of brain size in schizophrenia. These findings advance the understanding of cortical folding atypicalities in psychotic disorders.

Introduction

Early-life neurodevelopmental processes are thought to be aberrant in first-episode psychosis (FEP) and schizophrenia (SZ). This notion is corroborated by reported average reductions in the degree of folding and sulcation of FEP and SZ relative to healthy individuals (HIs) (Dazzan et al., 2021). However, the degree of folding is not static throughout life in HIs but reduces postnatally (Cao et al., 2017). Reductions in folding are associated with changes in gray and white matter morphology (Kochunov and Hong, 2014; Díaz-Caneja et al., 2021; Kochunov et al., 2022). Peak values of cortical thickness and fractional anisotropy differ by a decade, and peak fractional anisotropy values coincide with average age at onset of positive symptoms (Kochunov and Hong, 2014). Consequently, aging trends for morphologic metrics differ in normative and patient samples. Nevertheless, in older individuals with SZ, accelerated aging may occur simultaneously for gray and white matter and affect cortical folding (Kochunov and Hong, 2014; Kochunov et al., 2022).

Longitudinal studies can establish whether SZ is associated with progressive folding reductions. In addition, longitudinal studies can clarify whether SZ-related folding abnormalities can also occur at later stages of the illness during late adulthood and old age (Raznahan et al., 2011; Palaniyappan et al., 2013; Li et al., 2014; Libero et al., 2019).

The *in vivo* degree of folding can be estimated using the sulcation index (SI) (Shimony et al., 2016). SI combines two components: hull surface area (exposed cortex) and sulcal surface area (nonexposed cortex). Sulcal surface area can be decomposed into sulcal depth and length, thus decomposing the SI into folding subcomponents (Fig. 1) (Mangin et al., 2004). Assessing the SI and its subcomponents in a longitudinal lifespan study of HIs and individuals with SZ allows for a fine-grained assessment of change in folding across the lifespan and whether SZ contributes distinctively to the folding subcomponents.

Reduced total brain volume (TBV) is a robust neurobiological feature of psychotic disorders (Haijma et al., 2013). Since smaller brain sizes are associated with a lower degree of folding and early-life folding growth positively correlates with brain volume growth, the question arises whether reduced folding in psychotic disorders may be merely because of a global decrease in brain size (Toro et al., 2008). The relationship between brain size and folding metrics may be allometric (i.e., nonlinear) (Reardon et al., 2018), which can invalidate traditional covariate-based methods. Variability in folding can be related to factors affecting neurodevelopment (e.g., brain disorders) (Germanaud et al., 2014). Studying neurodevelopmental disorders, such as severe microcephalies, in an allometric context demonstrated that profound reductions of folding in patients could be fully explained by reduced brain volume. Meaningful associations of folding with disease may therefore only emerge after accounting for allometric scaling (Germanaud et al., 2014).

Allometric scaling laws predict that the static relationship between brain volume and areal measures (sulcal and hull area) in a log-log framework should be 2/3, whereas the relationship with linear measures (sulcal depth and length) should be 1/3 (Toro et al., 2008; Fish et al., 2017). However, the only study so far to assess scaling of brain volume with sulcal folding metrics in neurotypical children shows that larger brains have a higher SI because of a disproportionate increase in sulcal length but not depth (Fish et al., 2017). While interesting, it is unclear whether the observed allometric scaling also affects longitudinal trajectories of folding metrics and modulates potential differences in trajectories between SZ and HIs.

In this study, we first set out to replicate the previously reported normative scaling norms in two independent samples of HIs. Thereafter, we assess whether SZ or FEP groups differ from the HI group in allometric scaling. We then compare longitudinal age trajectories of folding metrics between SZ and HIs. Finally, we apply longitudinal allometric scaling to examine how change in folding subcomponents relates to change in TBV and whether this scaling differs between SZ and health.

Materials and Methods

Our study uses two independent samples (Sample 1, Sample 2) of humans. Detailed clinical, demographic, and imaging measures for both samples are summarized in Tables 1 and 2.

Sample 1: SZ and HIs (longitudinal)

From a large longitudinal sample of individuals with SZ and HIs 16-70 years of age at baseline, we included individuals who had T1-weighted MRI scan acquisitions at two or three time points. Detailed information regarding diagnostic criteria and clinical and cognitive assessments of the Utrecht Schizophrenia project and the Genetic Risk and Outcome of Psychosis consortium are described previously (Hulshoff Pol et al., 2001; Korver et al., 2012; Kubota et al., 2015). Detailed information on the current subsample can be found in Janssen et al. (2021). Details on the MRI quality assessment (both FreeSurfer and BrainVISA) and time between scans can be found in Díaz-Caneja et al. (2021). The final dataset consisted of 1087 scans from 298 HIs and 168 patients. Demographic, cognitive, and clinical information of the participants at all time points is summarized in Table 1, and information at baseline is summarized in Table 2 (left column). The study was approved by the institutional review board and was conducted according to the provisions of the World Medical Association Declaration of Helsinki. Written informed consent was obtained from all participants and also from parents/legal guardians for children under 18 years of age.

Sample 2: FEP and HIs (cross-sectional)

The sample is a subset of participants with available imaging data from a larger multisite, naturalistic study, including participants 7-35 years of

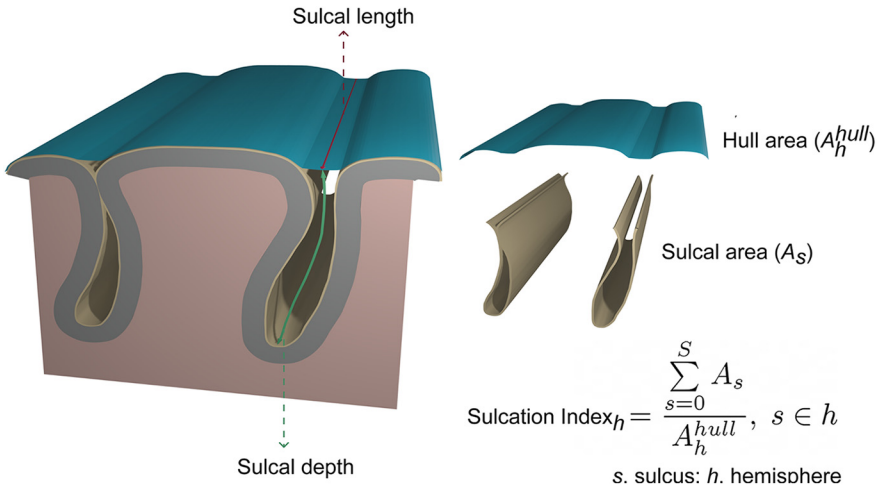

Figure 1. Graphical representation of SI and its components. Total sulcal surface area is defined as the sum of the area of all sulcal median meshes. Hull surface area is derived by calculating the area of the brain mesh defined via a morphologic closing of the brain mask, which excludes sulcal areas during definition of the exposed cortical surface area. Total sulcal length is measured on the hull and is defined as the summed distance of the intersections between the median sulcal surfaces and the hull. Geodesic sulcal depth is the shortest distance along the surface of the brain from the point to where the brain surface makes contact with the hull surface.

Table 1. Demographic, cognitive, and clinical characteristics of individuals with SZ and HIs for Sample 1[a]

	SZ patients			HIs		
No. of scans	Baseline (169)	Follow-up 1 (168)	Follow-up 2 (50)	Baseline (298)	Follow-up 1 (293)	Follow-up 2 (109)
Socio-demographics						
Sex, *n* (%), males	131 (77.51)	—	—	167 (56)	—	—
Age, years: mean (SD)	29.86 (9.27)	34 (9.55)	34.4 (5.75)	30.42 (10.96)	34.41 (10.96)	33.96 (8.10)
Education, years: mean (SD)	20.21 (25.7)	19.75 (24.9)	NA	21.75 (25)	20.19 (22.88)	NA
Cognitive and clinical variables						
Full-scale IQ total: mean (SD)	97.86 (16.5)	103 (20.22)	100.42 (18.58)	110.34 (15.74)	113.9 (16.5)	115.62 (17.6)
Age of onset, years: mean (SD)[b]	22.13 (5.28)	—	—			
Duration of illness, years: mean, (SD)[c]	6.32 (6.63)	11.04 (7.7)	11.84 (3.91)			
PANSS score, total: mean (SD)	63.34 (19.26)	50.18 (14.2)	56.2 (13.97)			
Total positive symptoms	14.96 (5.82)	12.37 (4.62)	13.26 (3.83)			
Total negative symptoms	16.27 (6.22)	12.87 (5.64)	15.22 (5.45)			
Total general symptoms	31.22 (11.2)	24.93 (7.02)	27.71 (7.28)			
Antipsychotics[d]						
Without medication, *n* (%)	7 (4.14)	7 (4.16)	NA			
Exclusively typical, *n* (%)	23 (13.6)	12 (7.14)	NA			
Exclusively atypical, *n* (%)	89 (52.66)	92 (54.76)	NA			
Both, *n* (%)	4 (2.36)	2 (1.19)	NA			
Cumulative dose exposure (mg): mean (SD)	275837.8 (397345.9)	945754.9 (1285851)	NA			
Missing, *n* (%)	103 (61.54)	102 (60.71)	50 (100)			

[a]The total amount of scans is 1087. PANSS, Positive and Negative Symptoms Scale.
[b]Age of onset is the age at which the first positive symptom occurs.
[c]Duration of illness is calculated based on the date of the appearance of first positive symptoms of SZ until the date of scan.
[d]Antipsychotic treatment data are not available for all the patients included (82 patients had medication information). Cumulative doses were calculated at the time of scan and given in chlorpromazine equivalents using standard conversion factors and estimated by the daily doses of each of the antipsychotics used by the patient.

age with a first episode of psychosis, the PEPs Project. The main objective of the PEPs Project was to identify the several gene × environment interactions involved in the risk of psychosis in a naturalistic cohort of FEP to develop a predictive model of psychosis. Most of the centers were integrated in the well-recognized Spanish network of research in Mental Health, "Centro de Investigación Biomédica en Red de Salud Mental." Detailed information about the study design, recruitment procedures, inclusion and exclusion criteria, clinical and cognitive assessments, and MRI quality assessment are provided previously (Bernardo et al., 2013; Pina-Camacho et al., 2016). For the current study, only participants scanned at a single site (Barcelona) were included ($n = 182$) of which a further 32 participants were excluded based on image quality. Detailed demographic, cognitive, and clinical information for the final sample is summarized in Table 2 (right column). The study was approved by the institutional review board and was conducted according to the provisions of the World Medical Association Declaration of Helsinki. Written informed consent was obtained from all participants and from parents/legal guardians for children under 18 years of age.

MRI acquisition

Image acquisition. For Sample 1, two scanners (same vendor, field strength and acquisition protocol) were used. Participants were scanned twice on either a Philips Intera or Achieva 1.5 T, and a T1-weighted, three-dimensional, fast-field echo scan with 160-180 1.2 mm contiguous coronal slices (TE, 4.6 ms; TR, 30 ms; flip angle, 30°; FOV, 256 mm; in-

Table 2. Demographic, cognitive and clinical variables of individuals with SZ or FEP and HIs of Samples 1 (at baseline) and 2[a]

	SZ patients ($n = 169$)	HIs ($n = 298$)
Socio-demographics		
Sex, *n* (%), males	131 (77.51)	167 (56)
Age, years: mean (SD)	29.86 (9.27)	30.42 (10.96)
Education, years: mean (SD)	20.21 (25.7)	21.75 (25)
Cognitive and clinical variables		
Full-scale IQ total: mean (SD)	97.86 (16.5)	110.34 (15.74)
Age of onset, years: mean (SD)[b]	22.13 (5.28)	
Duration of illness, years: mean, (SD)[c]	6.32 (6.63)	
PANSS score, total: mean (SD)	63.34 (19.26)	
Total positive symptoms	14.96 (5.82)	
Total negative symptoms	16.27 (6.22)	
Total general symptoms	31.22 (11.2)	
Antipsychotics[d]		
Without medication, *n* (%)	7 (4.14)	
Exclusively typical, *n* (%)	23 (13.6)	
Exclusively atypical, *n* (%)	89 (52.66)	
Both, *n* (%)	4 (2.36)	
Cumulative dose exposure per scan (mg): mean (SD)	27,5837.8 (39,7345.9)	
Missing, *n* (%)	103 (61.54)	
	FEP patients ($n = 89$)	HIs ($n = 61$)
Socio-demographics		
Sex, *n* (%), males	56 (70)	36 (62)
Age, years: mean (SD)	21.55 (4.66)	22.85 (5.14)
Cognitive and clinical variables		
Estimated IQ total: mean (SD)	92.40 (15.23)	106.58 (11.58)
Age of onset, years: mean (SD)[b]	20.83 (4.64)	
Duration of illness, years: mean, (SD)[c]	157.88 (109.6)	
PANSS score, total: mean (SD)	74.7 (21.68)	
Total positive symptoms	18.20 (7.6)	
Total negative symptoms	18.61 (8.15)	
Total general symptoms	37.89 (11.41)	
Antipsychotic use (AP)[d]		
Use of AP at scan, *n* (%)	74 (93%)	
Cumulative dose at scan (mg): mean (SD)	33,330.95 (40,504.16)	

[a]PANSS, Positive and Negative Symptoms Scale; AP, antipsychotic use.
[b]Age of onset is the age at which the first positive symptoms occurred.
[c]Duration of illness is calculated based on the date of the appearance of first positive symptoms of SZ until the date of scan.
[d]Antipsychotic treatment data are not available for all the patients included (82 patients had medication information). Cumulative doses were calculated per time of scan and given in chlorpromazine equivalents using standard conversion factors and estimated by the daily doses of each of the antipsychotics used by the patient.

plane voxel size, 1×1 mm^2) was acquired. All included participants had their baseline and follow-up scan on the same scanner. For Sample 2, participants were scanned on a Siemens Trio TIM 3 T, and a T1-weighted, three-dimensional, gradient echo scan with 240 1 mm contiguous sagittal slices (TE, 2.98 ms; TR, 2300 ms; flip angle, 9°; FOV, 256 mm; in-plane voxel size, 1×1 mm^2) was acquired.

Image analysis. TBV, SI, total sulcal and hull area, global average sulcal depth, and total sulcal length were assessed (Fig. 1). All images were analyzed using the FreeSurfer analysis suite (version 5.1) with default settings to provide total gray and white matter volumes, which were summed to calculate TBV (Dale et al., 1999; Fischl et al., 1999; Fischl, 2012). TBV was consistent across FreeSurfer version 5.1 and the more recent version 6.0. The intraclass correlation coefficient estimates and their 95% CIs based on a single-rating, consistency-agreement, two-way mixed-effects model for TBV was 0.988 (0.987-0.989) for Sample 1 and 0.994 (0.992-0.996) for Sample 2.

For all images, sulcal segmentation and identification were performed with BrainVISA software (version 4.5) using the Morphologist Toolbox and Mindboggle software using default settings (Mangin et al., 2004, 2010; Klein et al., 2017). After importing Freesurfer's ribbon image into BrainVISA, each sulcus is segmented with the cortical sulci corresponding to the crevasse bottoms of the "landscape," the altitude of which is defined by image intensity. A spherical hull surface was generated from a smooth envelope that wrapped around the hemisphere but did not encroach into the sulci; a morphologic isotropic closing of 6 mm was applied to ensure boundary smoothness. The median sulcal surface spans the entire space contained in a sulcus, from the fundus to its intersection with the hull. For each fold, sulcal area is defined as the total surface area of the medial sulcal surface, and sulcal length is measured on the hull and is defined as the length of the intersection between the median sulcal surface and the hull. All sulcal nodes belonging to a hemisphere were relabeled to one label, and then BrainVISA software was used to calculate hemispheric sulcal area and length. FreeSurfer output was imported into Mindboggle software for calculating geodesic sulcal fundi depth. All metrics were measured in the native space of the participant's images, and left and right hemisphere values were either summed or averaged. FreeSurfer-, BrainVISA-, and Mindboggle-derived measurements have been validated via histologic and manual measurements and have shown good test–retest reliability (Rosas et al., 2002; Kuperberg et al., 2003; Pizzagalli et al., 2020).

Statistics

All analyses were performed in R (https://cran.rstudio.com/).

Allometric analyses at baseline: Samples 1 and 2.

Normative scaling coefficients from HIs. We first regressed out the effects of age (age, age^2, age^3), sex, and scanner (only for Sample 1), by computing at each time point separately a linear regression model with each metric m as dependent variable and the covariates as predictors. To control for collinearity among the polynomials of age, we made use of the poly()-function in R, which created three uncorrelated variables to model age effects (so-called orthogonal polynomials) (34) for metric m (Chambers and Hastie, 1992) as follows:

$$m = \beta_0 + \beta_1(age) + \beta_2(sex) + \beta_3(scanner) \quad (1)$$

We then saved the residuals and added the mean back in for interpretability.

We converted the residualized metrics from HIs (Samples 1 and 2, separately) at baseline to log values and applied orthogonal regression to calculate normative baseline allometric scaling coefficients of log-transformed values of TBV with SI, sulcal and hull area, sulcal depth, and length. In our scenario, both dependent and independent variables have similar measurement error. Therefore, in our case, nonorthogonal regression may lead to biased regression estimates as only the measurement error of the independent variable is taken into account. In orthogonal regression, the measurement error of both dependent and independent variables is accounted for, leading to higher accuracy of regression estimates (Madansky, 1959). This method allowed us to assess whether the normative baseline allometric scaling relationships between the log transformed TBV and folding subcomponents were similar in the discovery sample (Sample 1) and the replication sample (Sample 2) and those reported by Fish et al. (2017) and whether they were similar compared with the expected scaling coefficients. The t for the difference between the observed and expected coefficients was calculated as follows:

$$t = \frac{(\beta_1 - \beta_{expected})}{se_\beta} \sim T(n_{HI} - 1) \quad (2)$$

where β_1 is the scaling coefficient for the HI group, $\beta_{expected}$ is the scaling coefficient as expected by scaling laws, se_β is the SE of the slope of the HI group given by bootstrapping, and n is the number of participants. For each folding metric, scaling coefficients below and above the expected values were considered to indicate hypoallometry and hyperallometry, respectively. Coefficients that were statistically indistinguishable from the null indicated isometric scaling. The *mcr* R package was used for orthogonal regression.

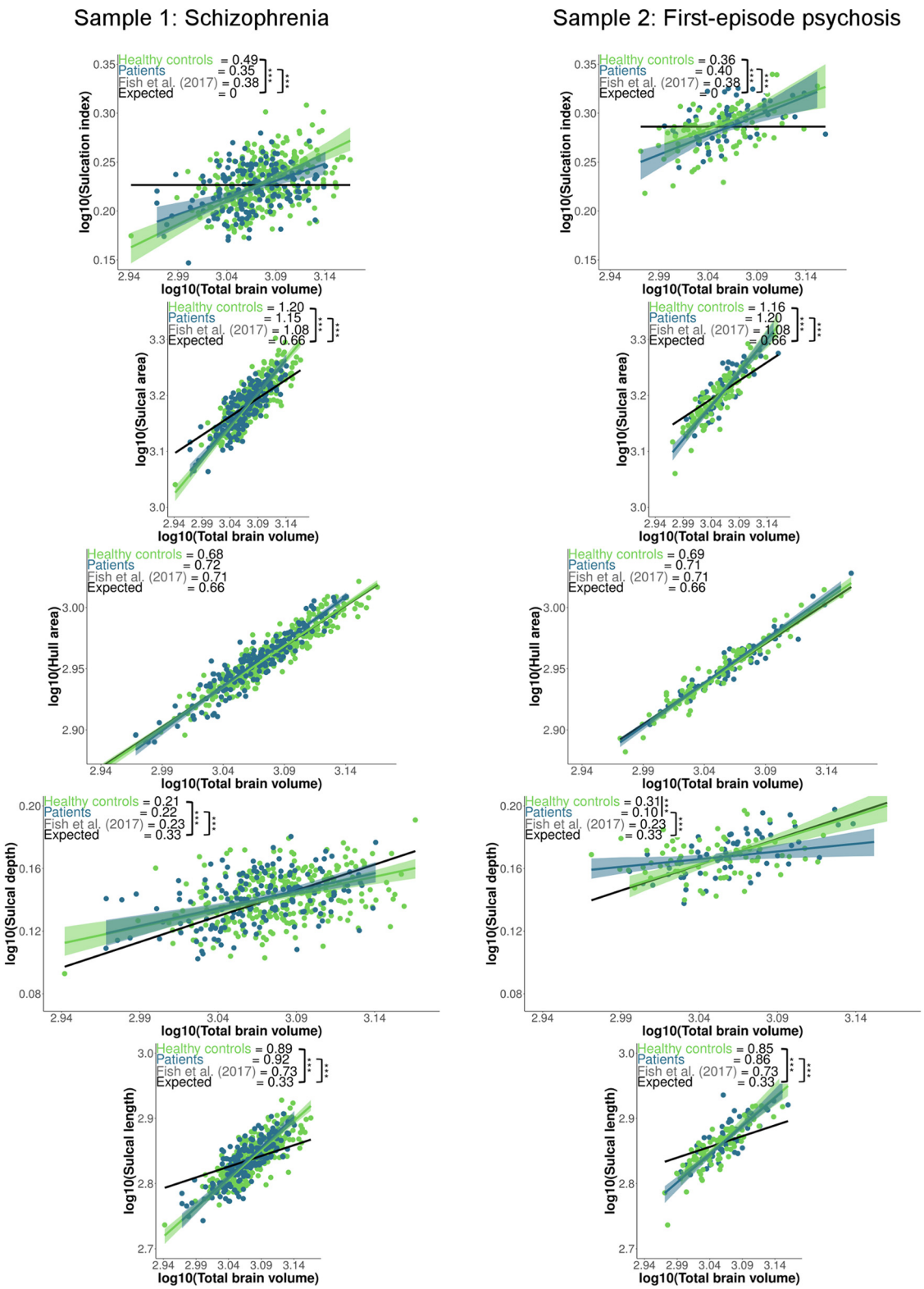

Figure 2. Orthogonal regression fits ± 95% CI and the scaling coefficient for observed log–log allometric scaling of residualized folding metrics relative to residualized TBV in the HI and patient groups at baseline (Samples 1 [left] and 2 [right] separately). "Expected" values (black line) represent the expected scaling (from scaling laws) coefficient. ***$p < 0.001$, significance after Bonferroni correction for the difference between (1) the scaling of the HI groups and the expected scaling and (2) the HI groups and patient groups. Values were residualized for scanner (only Sample 1), age, and sex.

Comparison of allometric scaling coefficients between HIs and SZ (Sample 1) and FEP (Sample 2). We converted the residualized metrics from SZ and FEP patients (Sample 1 and 2 separately) to log values and applied orthogonal regression to compare baseline allometric scaling coefficients between HIs and SZ (Sample 1) and FEP (Sample 2) separately. Significance of the slope was determined through 95% bias-corrected and accelerated bootstrap CIs generated using bootstrapping ($n = 1000$) (Efron and Tibshirani, 1993). If the slopes of the SZ

Table 3. Comparing different methods of controlling for brain size in analysis of diagnostic differences at baseline[a]

	SZ vs HIs	FEP vs HIs
SI		
Normalization	↑	—
Covarying	—	↓
Allometry	—	—
Sulcal area		
Normalization	—	—
Covarying	—	—
Allometry	—	—
Hull area		
Normalization	↑	↑
Covarying	↑	—
Allometry	—	—
Sulcal depth		
Normalization	↑	—
Covarying	—	—
Allometry	—	↓
Sulcal length		
Normalization	↑	—
Covarying	—	—
Allometry	—	—

[a]Folding metrics were compared between each patient group and their respective HI group using three different methods to control for TBV variation: normalizing by TBV, covarying by TBV, and within the allometric framework. Arrows indicate presence and direction of statistically significant group difference at $p < 0.05$.

and HI groups were both significant, we calculated a t for the difference between the slopes of the patient and HI groups, as follows:

$$t = \frac{(\beta_{patients} - \beta_{HI})}{se_{\beta}} \sim T(n_{patients} - 1) \quad (3)$$

where β_{HI} is the scaling coefficient for the HI group, $\beta_{patients}$ is the coefficient for the SZ group, se_{β} is the SE of the slope of the SZ group given by the bootstrap, and $n_{patients}$ is the number of patients.

In order to directly compare the results of our allometric approach to traditional methods of controlling for effects of TBV, we ran linear models comparing groups with expressing the residualized fold metrics as a fraction of TBV, that is, normalization, as follows:

$$residuals(m)/TBV = \beta_0 + \beta_1 \times diagnosis \quad (4)$$

and with adding TBV as a covariate,

$$residuals(m) = \beta_0 + (\beta_1 \times diagnosis) + (\beta_2 \times TBV) \quad (5)$$

where m is the metric.

Longitudinal age trajectories in SZ and HIs (Sample 1). We used generalized additive mixed models (GAMMs) to investigate the longitudinal trajectories of SI, sulcal and hull area, sulcal depth, and length over the age range (Wood, 2006). We specified cubic regression splines with shrinkage (a type of penalized splines) as smooth terms and set $k = 4$ as the number of knots of the spline. GAMM models were implemented to examine diagnosis (i.e., SZ vs HIs), the age × diagnosis interaction, and TBV, while controlling for sex and scanner (as fixed effects) and the random effect of the individual. Including a dummy variable to account for scanner type as a random effect in the models did not change the results. In order to account for the potential effect of a nonlinear relationship between cortical folding metrics and TBV on age trajectories, we reran the GAMM models but now transformed TBV and the folding metrics to log values. In these models, we also tested whether the log(TBV) × diagnosis interaction was significant. If this interaction was not significant, it was omitted from the model. To better understand the age × diagnosis interaction, GAMM estimates for age were also implemented and visualized for patients and HIs separately. We used the *mgcv* R package for modeling of the GAMMs. Finally, we plotted a difference fit (predicted SZ fit – predicted HIs fit) with its 95% CI against age. The difference fit allows for assessment of where along the age range the difference between SZ and HIs becomes significantly different from zero.

Longitudinal allometric analysis: the relationship between annual change in fold metrics and annual change in brain volume in SZ and HIs (Sample 1). In these analyses, we assessed whether yearly changes in folding metrics scaled with yearly changes in TBV and whether this scaling differed between the SZ and HI groups. For this, we used the residuals from baseline and the nearest available follow-up measurement from each subject to determine the symmetrized annual percent change (APC) for each subject and metric m as follows:

$$APC_m(a) = 100 \frac{1}{\bar{m}} \frac{\Delta m}{\Delta a} = 100 \frac{2}{a_i - a_{i-1}} \frac{m_i - m_{i-1}}{m_i + m_{i-1}}, \quad (6)$$

Where Δm represents change in metric m, obtained at two different time points, i and $i - 1$, $i \epsilon [2,3]$ (up to three measures per subject in this study) and Δa the time lapse between them in years; a is the subject's age in years at a specific time point. Finally, $\bar{m}$ represents the average of the metric's value at the two time points. We then calculated longitudinal allometric scaling coefficients of the APC of TBV versus the APCs of the folding metrics using orthogonal regression in HIs and individuals with SZ. Significance of the slope was determined through 95% bias-corrected and accelerated bootstrap CIs generated using bootstrapping ($n = 1000$) (Efron and Tibshirani, 1993). If the slopes of the SZ and HI groups were both significant, we calculated a t for the difference between the slopes of the patient and healthy participant group using the previously described formula (3).

In all analyses, we controlled for multiple comparisons using Bonferroni correction.

Results

Allometric analyses at baseline: Sample 1 and 2

Normative scaling coefficients from HIs

As can be seen in Figure 2, the cross-sectional allometric findings replicated across the two independent samples and replicated the normative findings reported by Fish et al. (2017). In the healthy participant groups of Sample 1 and 2, a larger SI was associated with a larger TBV. In both samples, there was hyperallometric scaling of SI, sulcal area and length, and isometric scaling of hull area. Sulcal depth showed either hypoallometric scaling (Sample 1) or isometric scaling (Sample 2).

Comparison of baseline allometric scaling coefficients between HIs and SZ (Sample 1) and FEP (Sample 2)

Allometric analyses indicated that, in both the SZ and FEP patient groups, the SI, sulcal and hull area, and sulcal length were in proportion with normative decreases in TBV (Fig. 2). Allometric analysis clearly demonstrated that SI, sulcal area, and sulcal length scaled nonlinearly with TBV in HIs, SZ, and FEP groups. Traditional methods of "controlling for" TBV differences, which assume linear scaling between the fold metrics and TBV, were not consistent with the results of our allometric analysis (Table 3). There were no significant associations between the residualized brain metrics, CPZ equivalents, and illness duration. In the group of SZ patients, estimated IQ explained ~9% of the variance of the brain metrics, except for sulcal depth (Fig. 3).

Longitudinal age trajectories in SZ and HIs (Sample 1)

There was no main effect of diagnosis for any of the metrics (Table 4). The healthy control and SZ group showed loss of TBV, sulcal area, and sulcal depth and length across the lifespan (Fig. 4*A*). After Bonferroni correction, the age × diagnosis

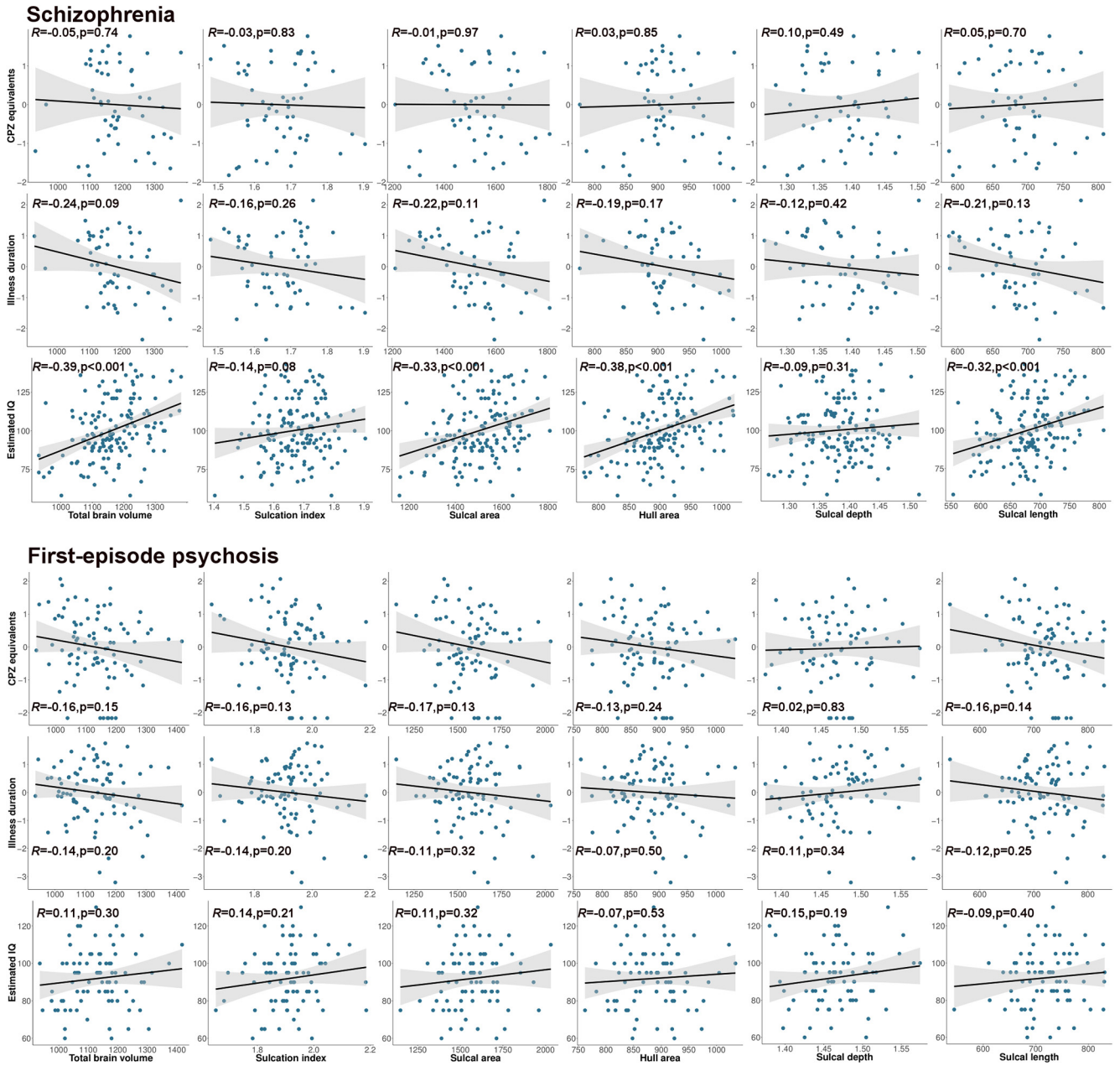

Figure 3. Regression plots for patients from Samples 1 and 2 showing the relationship between the brain measures at baseline and cumulative antipsychotics intake, illness duration, and estimated IQ. Chlorpromazine equivalents and illness duration were first normalized by selecting the optimal transformation method, based on the lowest Pearson *p* test statistic for normality, among the Yeo-Johnson, exp(x), log10, square-root, arcsinh, and orderNorm transformations (bestNormalize package, R). Participants missing data in Sample 1: cumulative antipsychotic usage (103), illness duration (60), and estimated IQ (44). Pearson correlations for each pair of variables were not significant after Bonferroni correction across samples. CPZ, Chlorpromazine equivalents.

interaction was significant for SI and sulcal area (Table 4). Trajectory differences in SI were >0 from 32 years onward approximately (approximate patient group deficit at 32 and at 61 years: −0.02 and −0.08, respectively) and for sulcal area from 44 years onward, approximately (approximate patient group deficit at 44 and at 61 years: –18 and –35 cm^2, respectively; see Fig. 4*B*).

Longitudinal allometric analysis: the relationship between annual change in fold metrics and annual change in brain volume in SZ and HIs

The APC of the hull area showed the strongest scaling with the APC of TBV, with no significant differences between the patient and control groups (Fig. 5). In the patient group, the scaling coefficient for the APC of SI and the APC of TBV (0.60) was similar to the scaling coefficient for the APC of sulcal area (0.63) and the APC of TBV. The patient group showed a significantly stronger scaling, that is, steeper slope for change in SI and sulcal area compared with the HI group (both *p* values < 0.001). There were no significant relationships for APCs of sulcal depth and length.

Discussion

Cross-sectional scaling of the SI, sulcal area, and sulcal length with TBV was significantly higher than expected (i.e., hyperallometric) in HIs, individuals with SZ, and those with FEP. There

Table 4. GAMM estimates for diagnosis and age × diagnosis for each brain metric in Sample 1[a]

Brain metrics	GAMM estimates							
TBV	Estimate		SE		*t*		*p*	
Diagnosis	−44.48		9.24		−4.82		<0.001[b]	
	edf		ref.df		*F*		*p*	
Age:patients	0.92		3		704.97		0.05	
SI	Estimate		SE		*t*		*p*	
	TBV	Log	TBV	Log	TBV	Log	TBV	Log
Diagnosis	−0.02	<−0.01	0.01	<0.01	−2.11	−2.05	0.04	0.04
	edf		ref.df		*F*		*p*	
Age:patients	1.34	1.39	3	3	642.66	741.41	<0.001[b]	<0.001[b]
Sulcal area	Estimate		SE		*t*		*p*	
Diagnosis	−8.36	<−0.01	7.86	<0.01	−1.06	−1.03	0.29	0.30
	edf		ref.df		*F*		*p*	
Age:patients	1.13	1.21	3	3	358.05	494.11	<0.01[b]	<0.01[b]
Hull area	Estimate		SE		*t*		*p*	
Diagnosis	3.01	<0.01	1.96	<0.01	1.54	1.51	0.12	0.13
	edf		ref.df		*F*		*p*	
Age:patients	1.21	2.71	3	3	942.27	1039.09	0.01	0.01
Sulcal depth	Estimate		SE		*t*		*p*	
Diagnosis	<0.01	<0.01	<0.01	<0.01	0.36	0.41	0.72	0.68
	edf		ref.df		*F*		*p*	
Age:patients	1.11	2.34	3	3	13.64	21.75	0.03	0.03
Sulcal length	Estimate		SE		*t*		*p*	
Diagnosis	−0.61	<−0.01	3.03	<0.01	−0.20	−0.21	0.84	0.83
	edf		ref.df		*F*		*p*	
Age:patients	0.16	0.42	3	3	0.84	6.63	0.26	0.20

[a]Two types of GAMMs were implemented: (1) TBV — with TBV, sex, and scanner as covariates; and (2) log — with log(TBV), sex, and scanner as covariates and predicting log(brain metric). Smooth function (edf), degrees of freedom (ref.df), and *F* statistics are given. Diagnosis is coded as an ordered factor (HIs = 0; patients = 1).
[b]*p* value indicates significance after Bonferroni correction.

were no diagnostic differences in scaling. Longitudinal analyses demonstrated steeper loss of SI and sulcal area through adulthood and beyond in SZ. Finally, we assessed the longitudinal allometric scaling between the APC of the folding metrics and the APC of TBV. The SZ group showed a significantly stronger scaling between the APC in SI and sulcal area with the APC of TBV compared with the HI group. This finding complemented our previous finding indicating that TBV changes over time are more strongly associated with changes in SI and sulcal area in SZ compared with HIs.

Allometric analyses at baseline: Sample 1 and 2

Normative scaling coefficients in HIs

The hyperallometric scaling of the SI with TBV was driven by a disproportionate expansion of sulcal area, with increasing TBV accompanied by a proportionate expansion of hull area. Allometric analysis revealed that disproportionate expansion of sulcal area with increasing TBV arises through a hyperallometric scaling relationship between TBV and sulcal length. This may be explained by an association between increased TBV and twistier sulci (Germanaud et al., 2012). Whether increased sulcal length in larger brains is also because of the presence of more ("new") sulci is difficult to assess. Currently, no common unified classification framework for sulci exists, complicating identification of "new" sulci (Ono et al., 1990; Mangin et al., 2010; Mikhael et al., 2018). It remains unclear what produces the hyperallometric scaling of TBV with sulcal surface area. Possible explanations include an expansion of the progenitor cell pool size producing an increased number of neurons during early-life neurodevelopment and/or as lineage regulation of the different types of cortical progenitors which mediate the tangential dispersion of radially migrating neurons (Llinares-Benadero and Borrell, 2019). The robustness of our normative findings is evidenced by the replication in an independent sample and replicating the scaling coefficients reported by Fish et al. (2017).

Comparison of baseline allometric scaling coefficients between HIs and SZ (Sample 1) and FEP (Sample 2)

Scaling relationships in FEP and SZ are in line with what is expected from the normative samples. Thus, disproportionate allometric scaling between TBV and SI, sulcal area, and length was also present in individuals with SZ and FEP. In other words, diagnostic differences in global sulcation and its determinants are proportional to the overall effect of diagnosis on TBV, with no added effect of diagnosis per se on these metrics. This suggests that, while a diagnosis of SZ or FEP is associated with decreased TBV, global aspects of cortical folding are not influenced by the illness. Only sulcal depth showed a different (hypoallometric) scaling in FEP compared with the normative samples. The reason for this is unclear, and this finding should be replicated in other FEP samples. Interestingly, results diverged when using classical methods for controlling for TBV which do not account for nonlinear relationships between the folding metrics and TBV, indicating that accounting for allometry matters when comparing global metrics of cortical folding between HIs and individuals with SZ or FEP.

Longitudinal age trajectories in SZ and HIs (Sample 1)

Our longitudinal analyses, to the best of our knowledge, provide the first evidence for diverging lifespan trajectories of SI and sulcal area in SZ compared with an HI group. After adjusting analyses for the effect of potential nonlinear relationships between cortical folding components and TBV on age trajectories, the SZ group demonstrated a steeper SI decline from ~32 years onward and a steeper sulcal area decline from

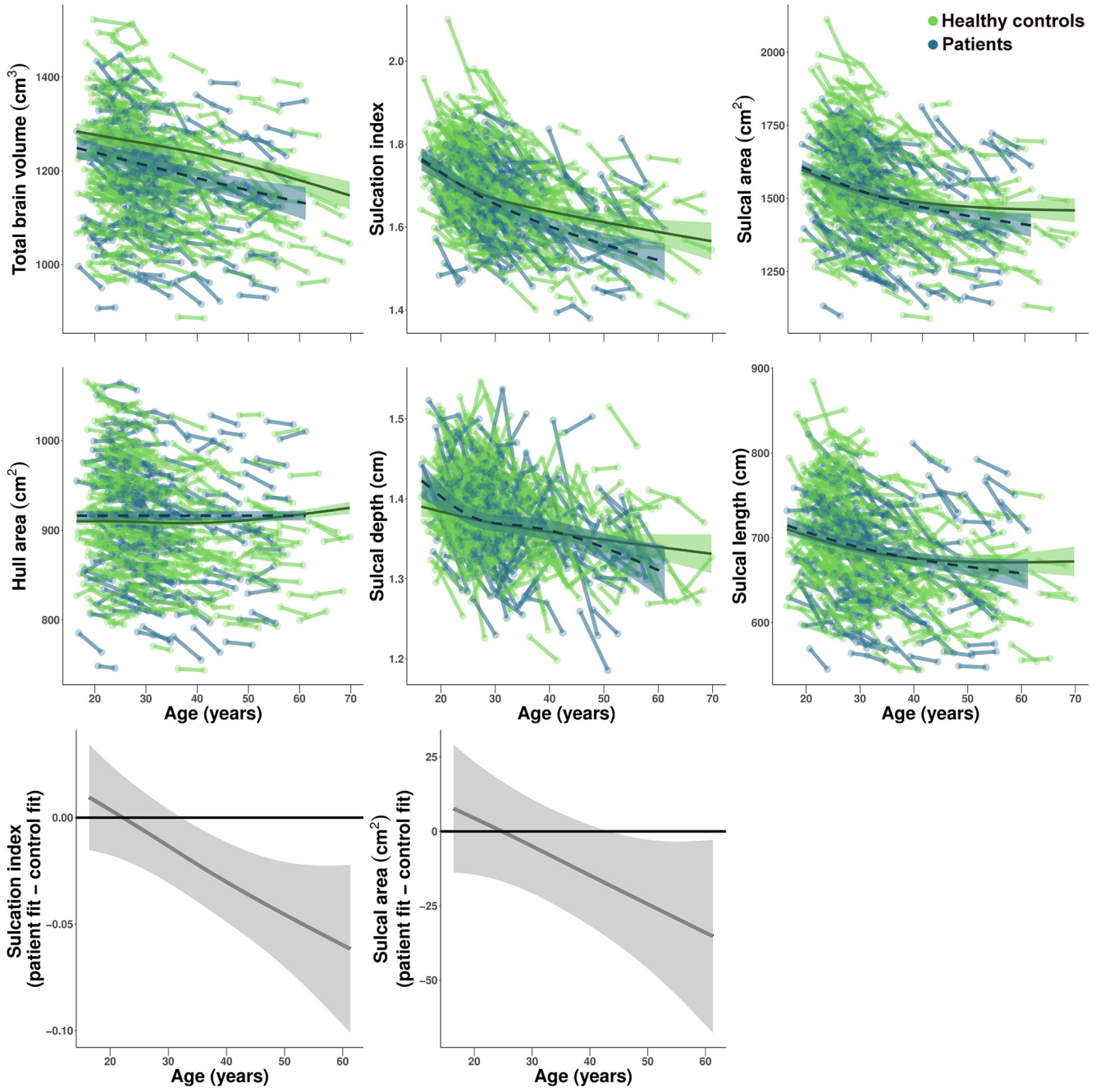

Figure 4. Age trajectories of sulcal metrics. Upper and middle rows, age trajectories of TBV and the five folding metrics in HIs and individuals with SZ from Sample 1. GAMM fits ± 95% CIs are shown over the data points for all participants in the corresponding color, with data at each of the time points connected for each participant. Sex, TBV, and scanner were included in the models as covariates (except for the model for TBV), and the individual was modeled as a random effect. SI and sulcal area showed a significant age × diagnosis interaction. Bottom row, difference fits ± 95% CI for SI and sulcal area. The plots display at approximately what age the mean difference between the predicted fits of the healthy participant and patient groups becomes different from zero and show that the mean difference between the diagnostic groups increases with age.

~44 years onward compared with the HI group. Our results are in line with increasing *in vivo* evidence for sulcal abnormalities associated with SZ. The amount of cortical surface area depends on cortical curvature. In SZ, sulcal curvature may be disproportionately decreased relative to gyral curvature (Wagstyl et al., 2016). In addition, age-dependent decreases in cortical thickness are more present in sulci than in gyri in HIs, and this effect may be more pronounced in SZ (Vandekar et al., 2015; Wagstyl et al., 2016). Supragranular layers (layers I-III) are thicker in sulci and thinner in gyri and thus possibly more vulnerable to excessive cortical thinning in SZ (Wagstyl et al., 2016); finally, there is consistent functional as well as postmortem evidence of supragranular layer pathology in SZ (Harrison and Weinberger, 2005; Williams and Boksa, 2010). Changes in hull surface area may be more sensitive to changes in gyri compared with sulci, and there were no differences in the age trajectories of hull surface area between the SZ and HI groups. Together, our results point to abnormal global sulcal changes over time in the SZ group. Sulcal heritability estimates and appearance of sulci during development are negatively correlated, implying that tertiary sulci, which are the latest to develop, may be under weaker genetic control compared with the preceding primary sulci (Pizzagalli et al.,

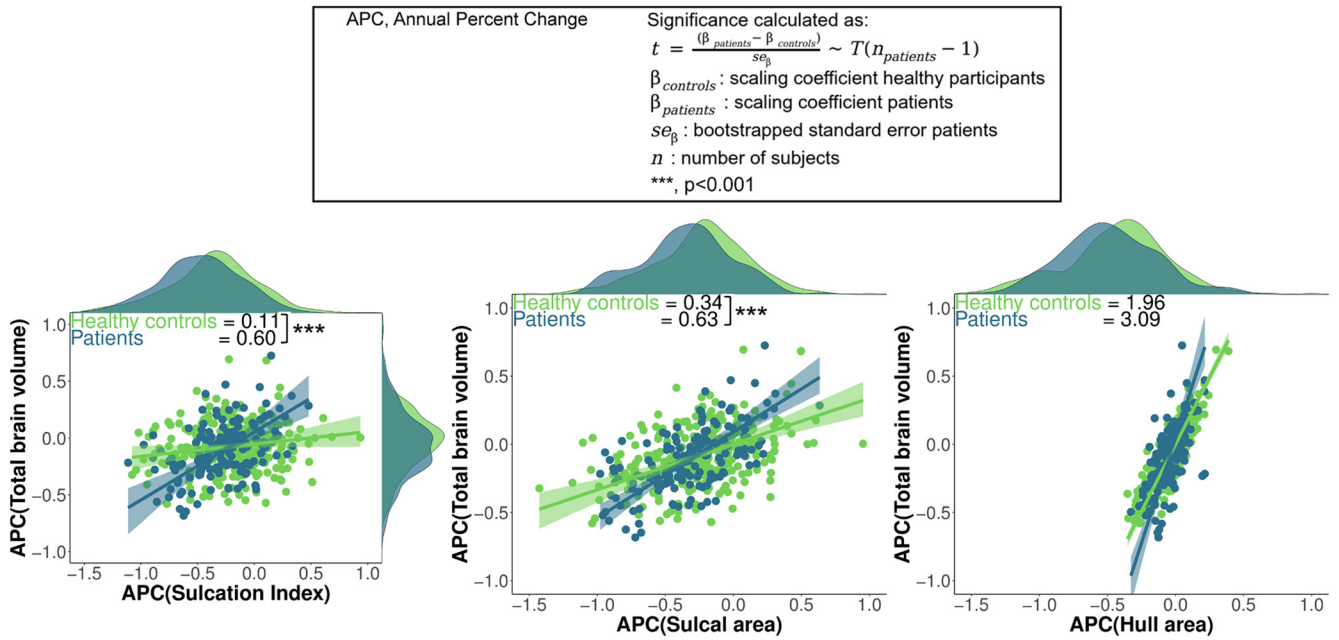

Figure 5. Orthogonal regression fits ± 95% CI and density maps for observed longitudinal allometric scaling of annual percent change of the folding metrics relative to the annual percent change of TBV in the HIs and the SZ patients in Sample 1. The formula for calculating whether the scaling coefficient differed between the HIs and patient groups is given. ***$p < 0.001$, significance after Bonferroni correction for the difference in scaling between the HI group and the patient group. APC values were estimated from values residualized for age, sex, and scanner.

2020). Longitudinal changes associated with SZ, such as progressive loss of gray matter and white matter integrity, could then have a stronger impact on tertiary sulci compared with primary sulci (Arango et al., 2012; Kochunov et al., 2016; Sun et al., 2016; Kelly et al., 2018; Sasabayashi et al., 2021). However, development of gray and white matter morphology is not synchronous; whole-brain white matter development is protracted by about a decade compared with gray matter development in individuals with SZ (Kochunov and Hong, 2014; Kochunov et al., 2022). In older adults, changes in white matter may become increasingly significant for reductions in cortical folding. Spectral analyses of folding in preterm and full-term newborns demonstrate that sulci largely develop in three overlapping successive waves (Dubois et al., 2019). Tertiary sulci are the last ones to develop around term age (Dubois et al., 2019). Spectral analysis further showed that development of tertiary sulci scaled hyper-allometrically with brain volume, which lends further support to the notion that development of tertiary sulci is associated with cortical expansion (Germanaud et al., 2012; Dubois et al., 2019). Tertiary sulci are also associated with myelination (Miller et al., 2021). Accelerated aging and its associated demyelination in individuals with SZ may reverse this process, decreasing the prominence of the tertiary sulci leading to a reduction in sulcal area and SI. Nevertheless, future longitudinal studies assessing gyral- and sulcal-specific morphology are necessary to determine whether aberrant morphologic changes over time are excessive in sulci compared with gyri.

Longitudinal allometric analysis: the relationship between annual change in fold metrics and annual change in brain volume in SZ and HIs

This study is the first to show the scaling between annual percent change in subcomponents of SI and change in TBV in HIs and individuals with SZ. We do not interpret the reported scaling coefficients from this longitudinal analysis as being hypo-, iso-, or hyper-allometric as there are, to the best of our knowledge, no prior studies presenting normative longitudinal scaling coefficients for folding subcomponents have been published. Scaling coefficients for SI and sulcal area were higher in the SZ group compared with the HI group; that is, TBV changes over time are more strongly associated with changes in SI and sulcal area in SZ compared with HIs. This complements our findings of the group differences in age trajectories. Loss of SI and sulcal area over time was higher in SZ, and this loss has an atypical strong association with change in TBV. As such, it may be that loss of SI and sulcal area, rather than hull area, sulcal depth, and length, are important contributors to the disproportionate loss of TBV over time in SZ.

A number of limitations should be taken into account when interpreting these findings. In Sample 1, antipsychotics usage information was heterogeneous and unfortunately limited. Thus, the obtained correlations between measures of chlorpromazine equivalents and brain metrics reported in this study are approximate, and the results must be interpreted cautiously. In FEP, sulcal depth scaled significantly less with TBV in patients compared with HIs. However, sulcal depth was the only metric for which this was the case, and this finding did not replicate across samples and should be replicated in future studies before interpreting this finding in a diagnostic context. Recent work demonstrated a power law relation between average global cortical thickness, total exposed cortical surface area, and total cortical surface area which describes the degree of folding (Wang et al., 2016). Whether this power law also predicts the relationship between the metrics used in the current study should be addressed in future studies. We assessed global but not regional (e.g., at the level of the individual sulcus) folding. By examining global aspects of cortical folding, we address brainwide geometric organization and, as such, provide a building block for future studies examining more local characteristics of folding.

References

Arango C, Rapado-Castro M, Reig S, Castro-Fornieles J, González-Pinto A, Otero S, Baeza I, Moreno C, Graell M, Janssen J, Parellada M, Moreno D, Bargalló N, Desco M (2012) Progressive brain changes in children and adolescents with first-episode psychosis. Arch Gen Psychiatry 69:16–26.

Bernardo M, Bioque M, Parellada M, Saiz Ruiz J, Cuesta MJ, Llerena A, Sanjuán J, Castro-Fornieles J, Arango C, Cabrera B, PEPs Group (2013) Assessing clinical and functional outcomes in a gene-environment interaction study in first episode of psychosis (PEPs). Rev Psiquiatr Salud Ment 6:4–16.

Cao B, Mwangi B, Passos IC, Wu MJ, Keser Z, Zunta-Soares GB, Xu D, Hasan KM, Soares JC (2017) Lifespan gyrification trajectories of human brain in healthy individuals and patients with major psychiatric disorders. Sci Rep 7:511.

Chambers JM, Hastie TJ (1992) Statistical models. S. Pacific Grove, CA: Wadsworth and Brooks/Cole.

Dale AM, Fischl B, Sereno MI (1999) Cortical surface-based analysis: I. Segmentation and surface reconstruction. Neuroimage 9:179–194.

Dazzan P, et al. (2021) Symptom remission and brain cortical networks at first clinical presentation of psychosis: the OPTiMiSE study. Schizophr Bull 47:444–455.

Díaz-Caneja CM, Alloza C, Gordaliza PM, Fernández-Pena A, de Hoyos L, Santonja J, Buimer EE, van Haren NE, Cahn W, Arango C, Kahn RS, Hulshoff Pol HE, Schnack HG, Janssen J (2021) Sex differences in lifespan trajectories and variability of human sulcal and gyral morphology. Cereb Cortex 31:5107–5120.

Dubois J, Lefèvre J, Angleys H, Leroy F, Fischer C, Lebenberg J, Dehaene-Lambertz G, Borradori-Tolsa C, Lazeyras F, Hertz-Pannier L, Mangin JF, Hüppi PS, Germanaud D (2019) The dynamics of cortical folding waves and prematurity-related deviations revealed by spatial and spectral analysis of gyrification. Neuroimage 185:934–946.

Efron B, Tibshirani RJ (1993) An introduction to the bootstrap. New York: Chapman and Hall.

Fischl B (2012) FreeSurfer. Neuroimage 62:774–781.

Fischl B, Sereno MI, Dale AM (1999) Cortical surface-based analysis: II. Inflation, flattening, and a surface-based coordinate system. Neuroimage 9:195–207.

Fish AM, Cachia A, Fischer C, Mankiw C, Reardon PK, Clasen LS, Blumenthal JD, Greenstein D, Giedd JN, Mangin JF, Raznahan A (2017) Influences of brain size, sex, and sex chromosome complement on the architecture of human cortical folding. Cereb Cortex 27:5557–5567.

Germanaud D, Lefèvre J, Fischer C, Bintner M, Curie A, des Portes V, Eliez S, Elmaleh-Bergès M, Lamblin D, Passemard S, Operto G, Schaer M, Verloes A, Toro R, Mangin JF, Hertz-Pannier L (2014) Simplified gyral pattern in severe developmental microcephalies? New insights from allometric modeling for spatial and spectral analysis of gyrification. Neuroimage 102:317–331.

Germanaud D, Lefèvre J, Toro R, Fischer C, Dubois J, Hertz-Pannier L, Mangin JF (2012) Larger is twistier: spectral analysis of gyrification (SPANGY) applied to adult brain size polymorphism. Neuroimage 63:1257–1272.

Haijma SV, van Haren N, Cahn W, Koolschijn PC, Hulshoff Pol HE, Kahn RS (2013) Brain volumes in schizophrenia: a meta-analysis in over 18,000 subjects. Schizophr Bull 39:1129–1138.

Harrison PJ, Weinberger DR (2005) Schizophrenia genes, gene expression, and neuropathology: on the matter of their convergence. Mol Psychiatry 10:40–68.

Hulshoff Pol HE, Schnack HG, Mandl RC, van Haren NE, Koning H, Collins DL, Evans AC, Kahn RS (2001) Focal gray matter density changes in schizophrenia. Arch Gen Psychiatry 58:1118–1125.

Janssen J, Díaz-Caneja CM, Alloza C, Schippers A, de Hoyos L, Santonja J, Gordaliza PM, Buimer EE, van Haren NE, Cahn W, Arango C, Kahn RS, Hulshoff Pol HE, Schnack HG (2021) Dissimilarity in sulcal width patterns in the cortex can be used to identify patients with schizophrenia with extreme deficits in cognitive performance. Schizophr Bull 47:552–561.

Kelly S, et al. (2018) Widespread white matter microstructural differences in schizophrenia across 4322 individuals: results from the ENIGMA Schizophrenia DTI Working Group. Mol Psychiatry 23:1261–1269.

Klein A, Ghosh SS, Bao FS, Giard J, Häme Y, Stavsky E, Lee N, Rossa B, Reuter M, Chaibub Neto E, Keshavan A (2017) Mindboggling morphometry of human brains. PLoS Comput Biol 13:e1005350.

Kochunov P, Hong LE (2014) Neurodevelopmental and neurodegenerative models of schizophrenia: white matter at the center stage. Schizophr Bull 40:721–728.

Kochunov P, Rowland LM, Fieremans E, Veraart J, Jahanshad N, Eskandar G, Du X, Muellerklein F, Savransky A, Shukla D, Sampath H, Thompson PM, Hong LE (2016) Diffusion-weighted imaging uncovers likely sources of processing-speed deficits in schizophrenia. Proc Natl Acad Sci USA 113:13504–13509.

Kochunov P, et al. (2022) Translating ENIGMA schizophrenia findings using the regional vulnerability index: association with cognition, symptoms, and disease trajectory. Hum Brain Mapp 43:566–575.

Korver N, Quee PJ, Boos HB, Simons CJ, de Haan L, GROUP Investigators (2012) Genetic Risk and Outcome of Psychosis (GROUP), a multi-site longitudinal cohort study focused on gene-environment interaction: objectives, sample characteristics, recruitment and assessment methods. Int J Methods Psychiatr Res 21:205–221.

Kubota M, van Haren NE, Haijma SV, Schnack HG, Cahn W, Hulshoff Pol HE, Kahn RS (2015) Association of IQ changes and progressive brain changes in patients with schizophrenia. JAMA Psychiatry 72:803–812.

Kuperberg GR, Broome MR, McGuire PK, David AS, Eddy M, Ozawa F, Goff D, West WC, Williams SC, van der Kouwe AJ, Salat DH, Dale AM, Fischl B (2003) Regionally localized thinning of the cerebral cortex in schizophrenia. Arch Gen Psychiatry 60:878–888.

Li G, Wang L, Shi F, Lyall AE, Lin W, Gilmore JH, Shen D (2014) Mapping longitudinal development of local cortical gyrification in infants from birth to 2 years of age. J Neurosci 34:4228–4238.

Libero LE, Schaer M, Li DD, Amaral DG, Nordahl CW (2019) A longitudinal study of local gyrification index in young boys with autism spectrum disorder. Cereb Cortex 29:2575–2587.

Llinares-Benadero C, Borrell V (2019) Deconstructing cortical folding: genetic, cellular and mechanical determinants. Nat Rev Neurosci 20:161–176.

Madansky A (1959) The fitting of straight lines when both variables are subject to error. J Am Stat Assoc 54:173–205.

Mangin JF, Rivière D, Cachia A, Duchesnay E, Cointepas Y, Papadopoulos-Orfanos D, Scifo P, Ochiai T, Brunelle F, Régis J (2004) A framework to study the cortical folding patterns. Neuroimage 23 Suppl 1:S129–S138.

Mangin JF, Jouvent E, Cachia A (2010) In-vivo measurement of cortical morphology: means and meanings. Curr Opin Neurol 23:359–367.

Mikhael S, Hoogendoorn C, Valdes-Hernandez M, Pernet C (2018) A critical analysis of neuroanatomical software protocols reveals clinically relevant differences in parcellation schemes. Neuroimage 170:348–364.

Miller JA, Voorhies WI, Lurie DJ, D'Esposito M, Weiner KS (2021) Overlooked tertiary sulci serve as a meso-scale link between microstructural and functional properties of human lateral prefrontal cortex. J Neurosci 41:2229–2244.

Ono M, Kubik S, Abernathey CD (1990) Atlas of the cerebral sulci. Stuttgart: Georg Thieme Verlag.

Palaniyappan L, Crow TJ, Hough M, Voets NL, Liddle PF, James S, Winmill L, James AC (2013) Gyrification of Broca's region is anomalously lateralized at onset of schizophrenia in adolescence and regresses at 2 year follow-up. Schizophr Res 147:39–45.

Pina-Camacho L, Del Rey-Mejías Á, Janssen J, Bioque M, González-Pinto A, Arango C, Lobo A, Sarró S, Desco M, Sanjuan J, Lacalle-Aurioles M, Cuesta MJ, Saiz-Ruiz J, Bernardo M, Parellada M, PEPs Group (2016) Age at first episode modulates diagnosis-related structural brain abnormalities in psychosis. Schizophr Bull 42:344–357.

Pizzagalli F, Auzias G, Yang Q, Mathias SR, Faskowitz J, Boyd JD, Amini A, Rivière D, McMahon KL, de Zubicaray GI, Martin NG, Mangin JF, Glahn DC, Blangero J, Wright MJ, Thompson PM, Kochunov P, Jahanshad N (2020) The reliability and heritability of cortical folds and their genetic correlations across hemispheres. Commun Biol 3:510.

Raznahan A, Shaw P, Lalonde F, Stockman M, Wallace GL, Greenstein D, Clasen L, Gogtay N, Giedd JN (2011) How does your cortex grow? J Neurosci 31:7174–7177.

Reardon PK, Seidlitz J, Vandekar S, Liu S, Patel R, Park MT, Alexander-Bloch A, Clasen LS, Blumenthal JD, Lalonde FM, Giedd JN, Gur RC, Gur RE, Lerch JP, Chakravarty MM, Satterthwaite TD, Shinohara RT, Raznahan A (2018) Normative brain size variation and brain shape diversity in humans. Science 360:1222–1227.

Rosas HD, Liu AK, Hersch S, Glessner M, Ferrante RJ, Salat DH, van der Kouwe A, Jenkins BG, Dale AM, Fischl B (2002) Regional and

progressive thinning of the cortical ribbon in Huntington's disease. Neurology 58:695–701.
Sasabayashi D, Takahashi T, Takayanagi Y, Suzuki M (2021) Anomalous brain gyrification patterns in major psychiatric disorders: a systematic review and transdiagnostic integration. Transl Psychiatry 11:176.
Shimony JS, Smyser CD, Wideman G, Alexopoulos D, Hill J, Harwell J, Dierker D, Van Essen DC, Inder TE, Neil JJ (2016) Comparison of cortical folding measures for evaluation of developing human brain. Neuroimage 125:780–790.
Sun Y, Chen Y, Lee R, Bezerianos A, Collinson SL, Sim K (2016) Disruption of brain anatomical networks in schizophrenia: a longitudinal, diffusion tensor imaging based study. Schizophr Res 171:149–157.
Toro R, Perron M, Pike B, Richer L, Veillette S, Pausova Z, Paus T (2008) Brain size and folding of the human cerebral cortex. Cereb Cortex 18:2352–2357.
Vandekar SN, Shinohara RT, Raznahan A, Roalf DR, Ross M, DeLeo N, Ruparel K, Verma R, Wolf DH, Gur RC, Gur RE, Satterthwaite TD (2015) Topologically dissociable patterns of development of the human cerebral cortex. J Neurosci 35:599–609.
Wagstyl K, Ronan L, Whitaker KJ, Goodyer IM, Roberts N, Crow TJ, Fletcher PC (2016) Multiple markers of cortical morphology reveal evidence of supragranular thinning in schizophrenia. Transl Psychiatry 6: e780.
Wang Y, Necus J, Kaiser M, Mota B (2016) Universality in human cortical folding in health and disease. Proc Natl Acad Sci USA 113:12820–12825.
Williams S, Boksa P (2010) Gamma oscillations and schizophrenia. J Psychiatry Neurosci 35:75–77.
Wood SN (2006) Generalized additive models: an introduction with R. Boca Raton, FL: Chapman Hall/CRC.